Available online at www.sciencedirect.com
SCIENCE DIRECT®
Journal of Geodynamics 39 (2005) 267–275
JOURNAL OF GEODYNAMICS
http://www.elsevier.com/locate/jog

Wavelet coherence analysis of Length-Of-Day variations and El Niño-Southern Oscillation

L.T. Liu [a,*], H.T. Hsu [a], E.W. Grafarend [b]

[a] *Institute of Geodesy and Geophysics, Chinese Academy of Sciences, Wuhan 430077, PR China*
[b] *Geodetic Institute, University of Stuttgart, Stuttgart 70174, Germany*

Received 20 July 2004; received in revised form 19 November 2004; accepted 20 November 2004

Abstract

Wavelet coherence analysis is defined and used to analyze the relationships between Length-Of-Day (LOD) variations and El Niño-Southern Oscillation (ENSO) on interannual scales. Using the newest observation data, this study quantitatively shows time-scale-dependent correlations and phase shifts between LOD variations and the ENSO. Good no-lag correlations (larger than 0.8) can be found on 3.0–4.9-year scales, while either obvious phase-shifts or low correlations are found on the other interannual scales. Around 2.5-year (biennial), 3.5-year and 5.0-year scales (i.e. around the time scales of ENSO's significant modes), the LOD variations with respect to the ENSO *lag* in phase by 4–5 months, *lead* by 3 months and *lag* by 3–5 months, respectively. Thus, there are obvious time-scale-dependent correlations and phase-shifts between the Earth rotation rate variations and the ENSO even within interannual scales.

Keywords: Wavelet coherence analysis; Length-Of-Day variations; El Niño-Southern Oscillation

1. Introduction

Length-Of-Day (LOD) variations, reflecting the changes in the solid Earth's axial rotation, are dynamic indicators of the motion and redistribution of the material inside or on the surface of the Earth. El Niño-Southern Oscillation (ENSO) is the most important coupled ocean–atmosphere phenomenon to cause

* Corresponding author. Tel.: +86 27 68881332; fax: +86 27 86783841.
E-mail address: llt@asch.whigg.ac.cn (L.T. Liu).

0264-3707/$ – see front matter © 2005 Elsevier Ltd. All rights reserved.
doi:10.1016/j.jog.2004.11.003

global climate variability on interannual scales, characterized by interannual oscillations in the tropical Pacific Sea Surface Temperature Anomaly (SSTA) and accompanied by large-scale fluctuations in air pressure occurring between the western and eastern tropical Pacific that are measured by the differences in air pressure anomaly between Tahiti and Darwin, Australia (i.e. the Southern Oscillation Index (SOI)). By the conservation of angular momentum, the ENSO changing the atmospheric angular momentum (AAM) can influence the solid Earth's angular momentum, leading to the varying LOD. Obvious relationships between the interannual LOD variations and the ENSO have been validated by many studies (Chao, 1984; Eubanks et al., 1986; Dickey et al., 1994). In fact, on interannual scales, the observed LOD variations are caused dominantly by the fluctuations in the atmospheric zonal winds (Hide and Dickey, 1991; Rosen, 1993). Seasonal LOD variations can be accounted for almost solely by the seasonal fluctuations in these atmospheric zonal winds (Rosen and Salstein, 1985). It is believed that the long-term (decadal to secular) variations in the LOD are caused by post-glacial rebound, core-mantle interaction, and tidal dissipation.

The ENSO shows several significant interannual modes around biennial and middle-interannual scales (Torrence and Compo, 1998). It has been reported that the correlations between LOD variations and the ENSO are poor on biennial scales (Chao, 1989). That means that the correlations may vary with time scale even within the interannual scales. Furthermore, the phases of the ENSO cycle do not exactly correspond to that of the LOD variations. Chao (1984) reported the finding that the SOI and the interannual LOD variations during 1957–1983 get a (negative) maximal correlation coefficient of -0.56 when the SOI leads in phase by 1 month; Eubanks et al. (1986) reported a maximal correlation coefficient during 1962–1984 of -0.5 when the SOI leads by 3 months; Chao (1988) reported a maximal correlation coefficient during 1972–1986 of -0.68 for a 2-month lead time; Dickey et al. (1993) reported a maximal correlation coefficient during 1964–1989 of -0.67 for a 1-month lead time. An interesting study shows that the ENSO signal can be detected by investigating the amplitude modulations of the seasonal LOD variations (Gross et al., 1996). The coherence studies mentioned above are done over entire interannual scales. In fact, the phase shifts between the LOD variations and the ENSO should vary with time scale even within the interannual scales. This study, defining a wavelet coherence analysis technique and using the newest observation data, will quantitatively investigate the correlations between the LOD variations and the ENSO with respect to time scale and phase shift.

2. Wavelet coherence analysis

Wavelet analysis is a useful mathematical technique for analyzing time signals of time-varying magnitudes and periodicities. The wavelet analysis has found many applications in studying the relationship between LOD variations and the ENSO (e.g. Gambis, 1992; Chao and Naito, 1995; Liu, 1999; Zhou et al., 2001). These studies comparing the continuous wavelet transform (CWT) of the LOD variations time series with that of the ENSO time series demonstrate that the LOD variations and the ENSO have similar spectral structures on interannual scales. Wavelet coherence analysis, which will be defined in the following, can provide further information about time-scale-dependent phase shifts and correlations between two different time signals. In other words, wavelet coherence analysis, based on wavelet transforms of two different time signals, provides a quantitative way to describe the correlations between two time signals as a function of both time scale and phase shift.

To define wavelet coherence analysis, we utilized wavelet amplitude-period spectrum (WAPS), a wavelet analysis technique initially developed to separate the Chandler wobble from the annual wobble

in the Earth's polar motion (Liu et al., 2000). For a time function $f(t) \in L^1(R)$, its WAPS is defined by

$$W_\psi f(a,b) = \frac{1}{c_\psi a}\int_{-\infty}^{+\infty} f(t)\psi\left(\frac{t-b}{a}\right)\mathrm{d}t, \quad a,b \in R, \quad a>0, \tag{1}$$

where a is time scale index and b is time translate index; $\psi(t) = \exp(-t^2/2\delta^2)\cos 2\pi t$ with δ being a real constant; and constant $c_\psi = \int \psi(t)\cos 2\pi t\,\mathrm{d}t$. Here $\psi(t)$ (real part of Morlet wavelet) is called the mother wavelet. The WAPS can be reviewed as an approximate version of the CWT. The advantage of the WAPS over the traditional CWT is that, for a time signal composed of some sinusoidal (or quasi-sinusoidal) sub-signals, its WAPS extremes can directly indicate sub-signals' local amplitudes and indices a and b of the extremes, respectively, indicate sub-signals' local periods and zero-phases (and π-phases). In other words, the WAPS of a time signal can directly recover the local amplitudes, periods and phase of the sub-signals contained in the time signal, which suggests the WAPS should be useful for coherence analysis. For the traditional CWT, that is not the case since it emphasizes on energy conservation other than amplitude maintenance.

For two time functions $f_1(t)$, $f_2(t) \in L^1(R)$, their *wavelet coherence* is defined by

$$c_{12}(a,s) = \frac{\int_{-\infty}^{+\infty} W_\psi f_1(a,b-s)W_\psi f_2(a,b)\mathrm{d}b}{\sqrt{\int_{-\infty}^{+\infty}|W_\psi f_1(a,b)|^2\mathrm{d}b}\sqrt{\int_{-\infty}^{+\infty}|W_\psi f_2(a,b)|^2\mathrm{d}b}}, \tag{2}$$

where s denotes the phase lag of $W_\psi f_2(a,b)$ versus $W_\psi f_1(a,b)$ at time scale a, which can be regarded as the phase lag of f_2(t) with respect to f_1(t) at time scale a. With time scale a fixed, WAPS $W_\psi f_1(a,b)$ as well as $W_\psi f_2(a,b)$ should fluctuate around zero as time translate b changes. That means, at a fixed time scale a, the $W_\psi f_1(a,b)$ as well as $W_\psi f_2(a,b)$ should have a mean (i.e. expectation value) of zero. Thus, the wavelet coherence function $c_{12}(a,s)$ as defined by Eq. (2) measures the correlation coefficient of time functions $f_1(t)$ and $f_2(t)$ when $f_2(t)$ lags $f_1(t)$ by s at time scale a. For instance, $c_{12}(a,0)$, called *no-lag wavelet coherence function* (NWCF), measures the correlation coefficient of $f_1(t)$ and $f_2(t)$ without any lag at time scale a. With time scale a fixed, there should be a maximal wavelet coherence as phase lag s ranges within $[-a/2, a/2]$, i.e., there should exist a function

$$\mathrm{Mc}_{12}(a) = \max\left\{c_{12}(a,s)|s \in \left[\frac{-a}{2},\frac{a}{2}\right]\right\}, \tag{3}$$

which is called *maximal wavelet coherence function* (MWCF). In fact the MWCF $\mathrm{Mc}_{12}(a)$ shows the maximal correction coefficient of time functions $f_1(t)$ and $f_2(t)$ at time scale a. The phase lag s that generates such maximal wavelet coherence indicates the phase shift between f_1(t) and $f_2(t)$ at time scale a. Generally, the sign of the MWCF should be uniformly positive. However, the MWCF can also be defined as the function of negative maximal wavelet coherences if one wants to check the anti-correlation between two time signals. In fact, a positive MWCF and a negative MWCF are equivalent in use for coherence studies, since there is only a phase-discrepancy of π between each other.

The process of computing the wavelet coherence function of two time signals and finding the MWCF is called a *wavelet coherence analysis* of the two time signals. A similar wavelet coherence analysis technique was developed and applied to the coherence analysis of seasonal LOD variations and AAM by Schmidt and Schuh (2000). In that analysis, they use the L^2-normalization CWT that interprets a

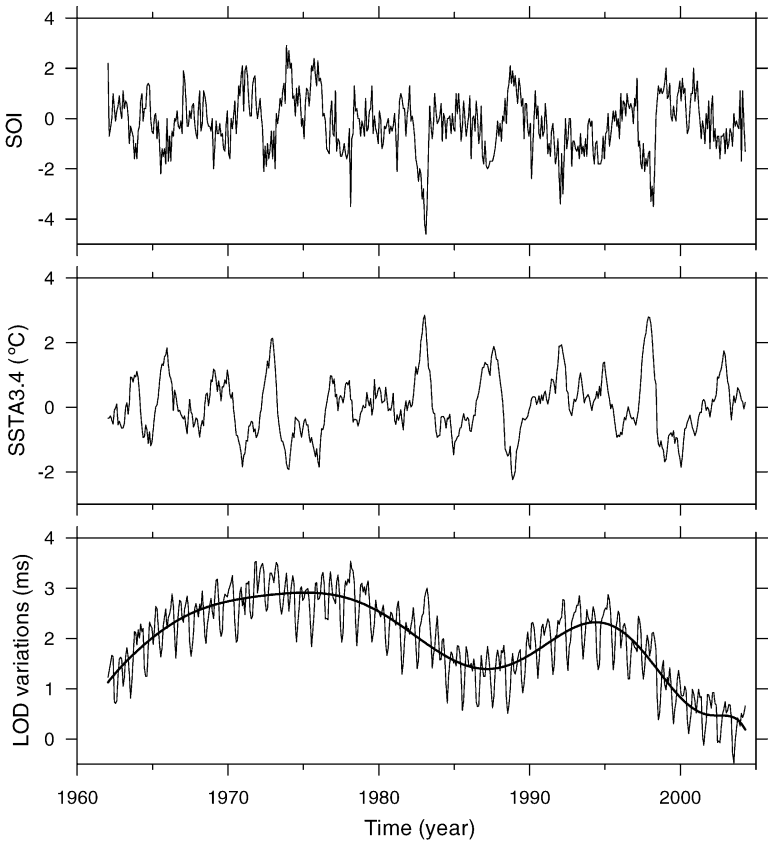

Fig. 1. Three monthly time series used in this study. SOI and SSTA3.4 come from the CPC, NCEP and LOD variations come from the EOPC04, IERRSS. Ten-degree polynomial fitted trend of the LOD variations is also shown (thick line).

time signal in terms of local energies but not local amplitudes. Here, we adopt the WAPS technique that interprets a time signal in terms of local amplitudes rather than energies.

3. Data and analysis experiments

Three monthly time series, SOI, SSTA3.4 and LOD variations, are prepared for this study (Fig. 1). All time series span the same time period of 1962–2004. The monthly SOI and SSTA3.4, two typical ESNO time series, are downloaded from the Climate Prediction Center (CPC), National Center for Environmental Prediction (NCEP). The LOD data come from the daily EOPC04, International Earth Rotation and Reference Systems Service (IERRSS). To enable the comparison with the monthly meteorological series, we have converted the daily EOPC04 values to monthly series by block averaging. The secular trend of the LOD is determined by a 10-degree polynomial fitting and is removed. The remaining forms the monthly LOD variations. To avoid any artificial filtering error, the significant annual term and semi-annual term in the LOD variations are not filtered out.

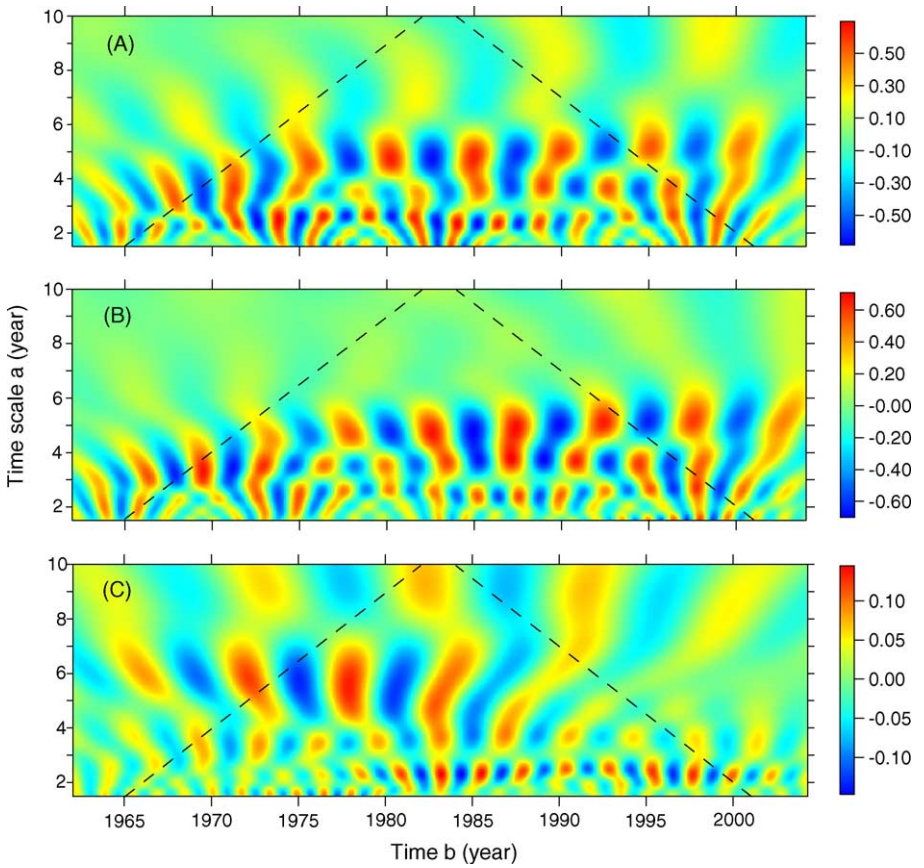

Fig. 2. Interannual wavelet amplitude-period spectra (WAPS) of SOI (A), SSTA3.4 (B) and LOD variations (C). Dashed lines denote edge-effect regions.

Two wavelet coherence analysis experiments are carried out. The first experiment is a wavelet coherence analysis of the SOI and the SSTA3.4 on interannual scales. It is very well known that the SOI and the SSTA are highly anti-correlated to each other on the interannual time scales (e.g. Philander, 1990; Nuzhdina, 2002). So there should be almost no phase-discrepancies between each other and their no-lag wavelet coherences should be very close to -1. Thus, results of this analysis experiment can test the effectiveness of the wavelet coherence analysis defined in Section 2. In the mean time, such an experiment can also show the major interannual modes in the ENSO cycle. The second experiment is a wavelet coherence analysis of the LOD variations and the SSTA3.4 on the interannual scales. This experiment quantifies the correlations between the LOD variations and the ENSO with respect to time scale and phase shift, and will provide the major results of this study.

In the first experiment, the SOI and the SSTA3.4 are, respectively, transformed into interannual WAPSes by allowing $\delta = 2^{1/2}$ and $a \in [1.5, 10]$ (Fig. 2A and B). One should note that the variable a of the WAPS serves as an exact indicator of period and that the radius (e-folding time) of the cone of influence (or edge effect region) is exactly $2a$ ($=2^{1/2}\delta a$) (Torrence and Compo, 1998). It is obvious that the WAPS of the SOI is very similar to that of the SSTA3.4 but in an anti-phase way. Extremes of the two WAPSes match well

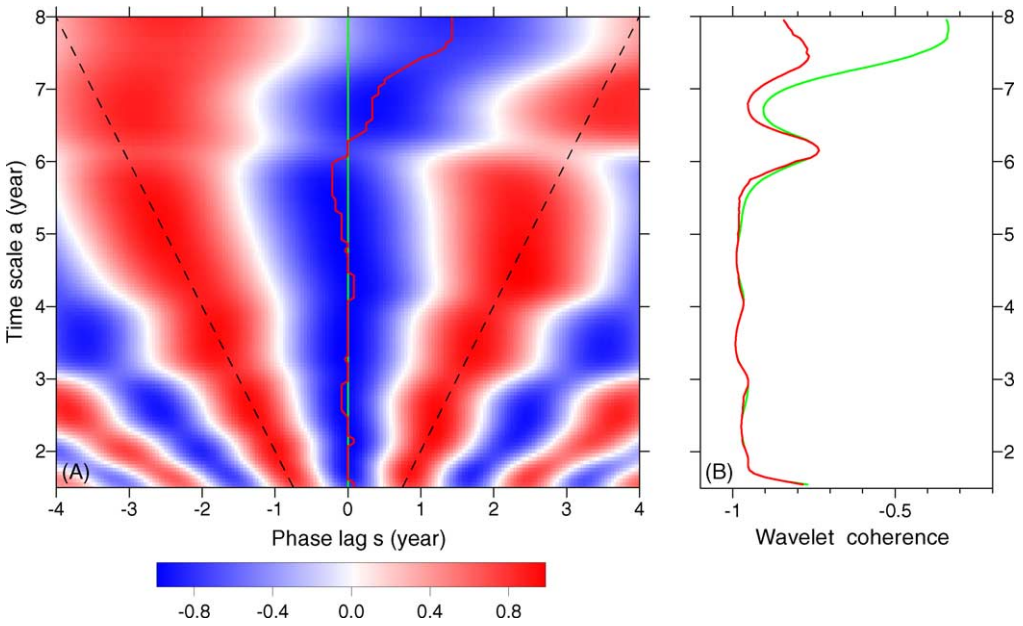

Fig. 3. Results of the wavelet coherence analysis of the SSTA3.4 vs. the SOI. (A) Wavelet coherence function $c_{\mathrm{SOI,SSTA3.4}}(a, s)$ in image. Red line denotes the trace of the MWCF and dashed lines denote the range of $[-a/2, a/2]$. (B) MWCF (red) and NWCF (green).

to each other in magnitude throughout the time span 1962–2004 and throughout the interannual scales. Both WAPSes clearly show three significant interannual modes, respectively, around biennial, 3.5-year and 5.0-year scales. The wavelet coherence function is then computed with a ranging within [1.5, 8] (Fig. 3A). The WAPS values within the edge effect regions are not used in the computations. Note that the edge-effect regions are very wide as the time scale a is larger than 8 years. The (negative) MWCF is then determined according to Eq. (3) by searching the wavelet coherence function for the deepest blue valley (Fig. 3B). The NWCF is also shown there.

The second analysis experiment is done just like the first one. We make a computation of the WAPS of the LOD variations, still with $\delta = 2^{1/2}$ (Fig. 2C). From Fig. 2B and C, one can observe that the WAPS extremes of the LOD variations match those of the SSTA3.4 only to some degree, and there are still obvious phase discrepancies. Then the wavelet coherence function is computed (Fig. 4A). The MWCF is determined according to Eq. (3) by searching the wavelet coherence function for the highest red ridge (Fig. 4B). The NWCF is also shown.

4. Results and discussions

Results of the first wavelet coherence analysis experiment verify the high anti-correlation between the SOI and the SSTA (Fig. 3). Throughout time scales of 1.5–7.0 years, the MWCF is very close to the NWCF with their values being very close to −1. The trace of the MWCF is also quite close to zero phase lag, with a standard deviation of 1.7 months within the time scale of 1.5–7.0 years. These results also

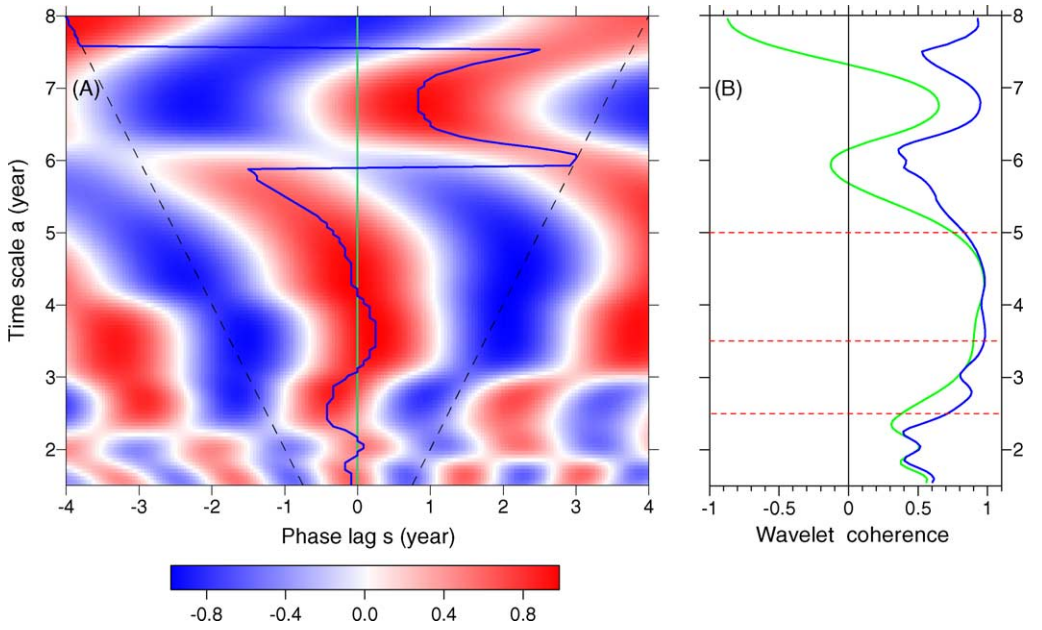

Fig. 4. Results of the wavelet coherence analysis of the SSTA3.4 vs. LOD variations. (A) Wavelet coherence function $c_{\mathrm{LOD,SSTA3.4}}(a, s)$ in image. Blue line denotes the trace of the MWCF and dashed lines denote range of $[-a/2, a/2]$. (B) MWCF (blue) and NWCF (green). Three dashed red lines denote the time scales of ENSO's significant modes.

verify the effectiveness of the wavelet coherence analysis defined in Section 2 in detecting the correlations with respect to time scale and phase lag.

The second wavelet coherence analysis experiment quantifies the correlations between LOD variations and SSTA3.4 with respect to time scale and phase lag (Fig. 4). One can see that the values of the MWCF, being around 0.5 or larger, obviously vary with time scale. This means that the LOD variations do correlate to the ENSO and such correlations are obviously time-scale-dependent. On 2.2–3.0-year and 5.0–8.0-year scales, the trace of the MWCF significantly differs from that of the NWCF (Fig. 4A), indicating large phase-discrepancies between the LOD variations and the ENSO on these time scales. On 1.5–2.2-year scales, both the MWCF and the NWCF are valued as low as about 0.5, not suggesting very good correlations. Only on 3.0–4.9-year scales the MWCF and the NWCF coincide well with each other with their values larger than 0.8, which reveals that the good correlations between the LOD variations and the ENSO mainly lie in the 3.0–4.9-year scales. Fig. 4 also shows a particular phenomenon: the LOD variations may correlate to the ENSO very well at 6.8-year scale, around which the maximal wavelet coherences are larger than 0.9. However, at this time scale, the LOD variations obviously lead the ENSO in phase by 10 months. As shown by the first wavelet coherence analysis experiment, the ENSO magnitudes are significant around the biennial, 3.5- and 5.0-year scales. So it is interesting to investigate the correlations between the LOD variations and SSTA3.4 around these three time scales. According to Fig. 4A, the LOD variations with respect to the SSTA3.4 lag in phase by about 4–5 months around the biennial scales, lead by about 3 months at the 3.5-year scale and lag by about 3–5 months at the 5.0-year scale. Thus, on the time scales around which the ENSO is significant in magnitude, the phase-discrepancies (including both phase lag and phase lead) between the LOD variations and the ENSO are still obvious.

The correlation between LOD variations and the SOI is not studied here. Figs. 3 and 4 suggest that this would be not useful since the outcome would be identical for $a < 7$ years. We do not investigate the correlation between LOD variations and the SOI for $a > 7$ years, since the degree of freedom in the coherence analysis decreases as a increases and degrades the credibility of the coherence analysis results.

Results of the second wavelet coherence experiment reveal that the interannual LOD variations do correlate to the ENSO because their maximal wavelet coherences are around 0.5 or larger throughout the interannual scales. Good correlations between the LOD variations and the ENSO mainly lie in 3.0–4.9-year scales. However, the interannual LOD variations can be explained only to some degree by the ENSO, since there are either obvious time-scale-dependent phase shifts or low correlations between each other on most of the interannual scales. Particularly, the LOD variations with respect to the ENSO lag in phase around the biennial and 5.0-year scales but lead in phase around the 3.5- and 6.8-year scales.

Acknowledgements

This study is supported by Alexander von Humboldt Research Fellowship and NSFC40174006.

References

Chao, B.F., Naito, I., 1995. Wavelet analysis provides a new tool for studying Earth's rotation. EOS, Trans. Am. Geophys. Union 76, 161–165.

Chao, B.F., 1988. Correlation of interannual length-of-day variation with El Niño/southern oscillation, 1972–1986. J. Geophys. Res. 93, 7709–7715.

Chao, B.F., 1984. Interannual length-of-day variation with relation to the southern oscillation/El Niño. Geophys. Res. Lett. 11, 541–544.

Chao, B.F., 1989. Length-of-day variations caused by El Niño-southern oscillation and quasi-biennial oscillation. Science 243, 923–925.

Dickey, J.O., Marcus, S.L., Eubanks, T.M., Hide, R., 1993. Climate studies via space geodesy: relationships between ENSO and interannual LOD variations. In: McBean, G.A., Hantel, M. (Eds.), Interactions between Global Climate, Systems: The Legacy of Hann, Geophys. Mono. Ser., vol. 75. AGU, Washington, DC, pp. 141–155.

Dickey, J.O., Marcus, S.L., Eubanks, T.M., Hide, R., 1994. Climate Studies via Space Geodesy: Relationships between ENSO and Interannual Length-of-day Variations, Fluxes of Matter between Global Climate Subsystems. American Geophysical Union Monograph.

Eubanks, T.M., Steppe, J.A., Dickey, J.O., 1986. The EL Niño, the southern oscillation, and the Earth's rotation. In: Cazenave, A. (Ed.), Earth Rotation: Solved and Unsolved Problems. D. Reidel, Hingham, MA, pp. 163–186.

Gambis, D., 1992. Wavelet transform analysis of the length of the day and El Niño/southern oscillation variations at intraseasonal and interannual time scales. Ann. Geophys. 10, 429–437.

Gross, R.S., Marcus, S.L., Eubanks, T.M., Dickey, J.O., Keppenne, C.L., 1996. Detection of an ENSO signal in seasonal length-of-day variations. Geophys. Res. Lett. 23, 3373–3376.

Hide, R., Dickey, J.O., 1991. Earth's variable rotation. Science 253, 629–637.

Liu, L.T., Hsu, H.T., Gao, B.X., Wu, B., 2000. Wavelet analysis of the variable Chandler wobble. Geophys. Res. Lett. 27 (18), 3001–3004.

Liu, L.T., 1999. Basic wavelet theory and its applications in Geodesy. Doctoral Thesis. Institute of Geodesy and Geophysics, Chinese Academy of Sciences, 110 pp.

Nuzhdina, M.A., 2002. Connection between ENSO and phenomena and solar and geomagnetic activity. Nat. Hazard Earth Syst. Sci. 2, 83–89.

Philander, S.G.H., 1990. El Niño La Niña and the Southern Oscillation. Academic Press, San Diego, CA, 289.

Rosen, R.D., Salstein, D.A., 1985. Contributions of stratospheric winds to annual and semiannual fluctuations in atmospheric angular momentum and the length of day. J. Geophys. Res. 90, 8033–8041.
Rosen, R.D., 1993. The axial momentum balance of the Earth and its fluid envelope. Surv. Geophys. 14, 1–29.
Schmidt, M., Schuh, H., 2000. Frequency-dependent phase lags between LOD- and AAM-variations detected by wavelet analysis. XXV EGS Gen. Ass., Nice, France, 25–29.04.
Torrence, C., Compo, G.P., 1998. A practical guide to wavelet analysis. Bull. Am. Meteorol. Soc. 79 (1), 61–78.
Zhou, Y.H., Zheng, D.W., Liao, X.H., 1998. Wavelet analysis of interannual LOD, AAM and ENSO: 98 El Niño and 99 La Niña signals. J. Geodesy. 75 (2–3), 164–168.